Template-Assisted Mechanosynthesis Leading to Benchmark Energy Efficiency and Sustainability in the Production of Bifunctional Fe-N-C Electrocatalysts

Kosimov, Akmal; Alimbekova, Amina; Assafrei, Jurgen Martin; Ahmadi, Majid; Roohi, Khatereh; Taheri, Peyman; Pinto, Sara M.; Cepitis, Ritums; Baptista, Antonio J.; Kongi, Nadezda

DOI
10.1021/acssuschemeng.3c02077

Publication date
2023

Document Version
Final published version

Published in
ACS Sustainable Chemistry and Engineering

ACS Sustainable Chemistry & Engineering

pubs.acs.org/journal/ascecg

Research Article

Template-Assisted Mechanosynthesis Leading to Benchmark Energy Efficiency and Sustainability in the Production of Bifunctional Fe−N−C Electrocatalysts

Akmal Kosimov, Amina Alimbekova, Jurgen-Martin Assafrei, Gulnara Yusibova, Jaan Aruväli, Maike Käärik, Jaan Leis, Päärn Paiste, Majid Ahmadi, Khatereh Roohi, Peyman Taheri, Sara M. Pinto, Ritums Cepitis, Antonio J. Baptista, Patrick Teppor, Enn Lust, and Nadezda Kongi*

Cite This: *ACS Sustainable Chem. Eng.* 2023, 11, 10825−10834

Read Online

ACCESS | Metrics & More | Article Recommendations | Supporting Information

ABSTRACT: Efficient and sustainable synthesis of performant metal/nitrogen-doped carbon (M−N−C) catalysts for oxygen reduction and evolution reactions (ORR/OER) is vital for the global switch to green energy technologies−fuel cells and metal−air batteries. This study reports a solid-phase template-assisted mechanosynthesis of Fe−N−C, featuring low-cost and sustainable $FeCl_3$, 2,4,6-tri(2-pyridyl)-1,3,5-triazine (TPTZ), and NaCl. A NaCl-templated Fe-TPTZ metal−organic material was formed using facile liquid-assisted grinding/compression. With NaCl, the Fe-TPTZ template-induced stability allows for a rapid, thus, energy-efficient pyrolysis. Among the produced materials, 3D-FeNC-LAG exhibits remarkable performance in ORR ($E_{1/2}$ = 0.85 V and E_{onset} = 1.00 V), OER ($E_{j=10}$ = 1.73 V), and in the zinc−air battery test (power density of 139 mW cm^{-2}). The multilayer stream mapping (MSM) framework is presented as a tool for creating a sustainability assessment protocol for the catalyst production process. MSM employs time, cost, resource, and energy efficiency as technoeconomic sustainability metrics to assess the potential upstream impact. MSM analysis shows that the 3D-FeNC-LAG synthesis exhibits 90% overall process efficiency and 97.67% cost efficiency. The proposed synthetic protocol requires 2 times less processing time and 3 times less energy without compromising the catalyst efficiency, superior to the most advanced methods.

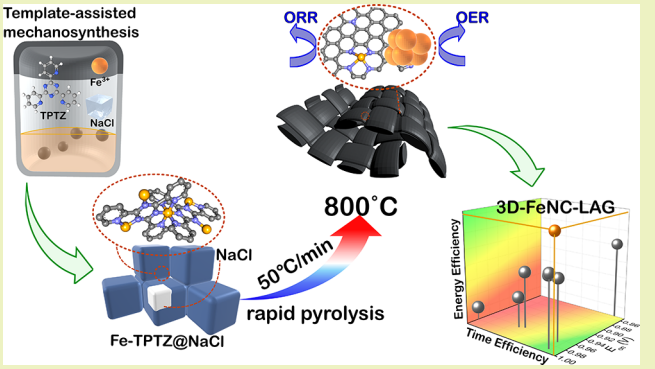

KEYWORDS: *M−N−C catalyst, template-assisted mechanosynthesis, oxygen electrocatalysis, zinc−air battery, sustainable synthesis*

INTRODUCTION

Electrochemical energy storage and conversion (ESC) devices, such as metal−air batteries (MABs) and fuel cells, have emerged as excellent replacements for fossil-based technologies, enabling the transition to more viable energetics.[1−3] Fuel cells and MABs can potentially reduce the mismatch between supply and demand while providing reliable, low-cost, portable, and clean energy sources without significant compromises in efficiency and energy density.[4] However, the principal mechanisms of these devices−electrochemical oxygen reduction and evolution reactions (ORR and OER, respectively) determine their overall performance and significantly impede progress due to their sluggish kinetics.

To achieve sufficient ORR/OER activity, state-of-the-art catalysts heavily rely on platinum group metals (PGMs).[5] However, high cost, scarcity, and poor durability of PGMs delay the further industry-scale application of ESC devices. Therefore, nonprecious metal catalysts (NPMCs) emerged as potential alternatives for PGMs.[6] More specifically, metal-nitrogen-doped carbon (M−N−C) materials stand out with their promising electroactivity, low cost, and a wide variety of sources.[7] The intelligent design of M−N−C materials (the choice of the M−N−C precursor, synthetic approach, and postsynthetic treatment) is a cornerstone of achieving efficient ORR and OER, which provides a versatile platform to reach exceptional catalytic performance.[7] Many studies have successfully attained the bifunctionality of M−N−C materials by merging ORR-active single-atom sites (SASs) and OER-active nanoparticles within a sole carbon matrix.[8]

Nevertheless, the liquid-phase-reliant synthetic protocols of M−N−C catalysts (e.g., precipitation, deposition−precipita-

Received: April 8, 2023
Revised: June 13, 2023
Published: July 11, 2023

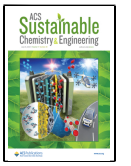

https://doi.org/10.1021/acssuschemeng.3c02077
ACS Sustainable Chem. Eng. 2023, 11, 10825−10834

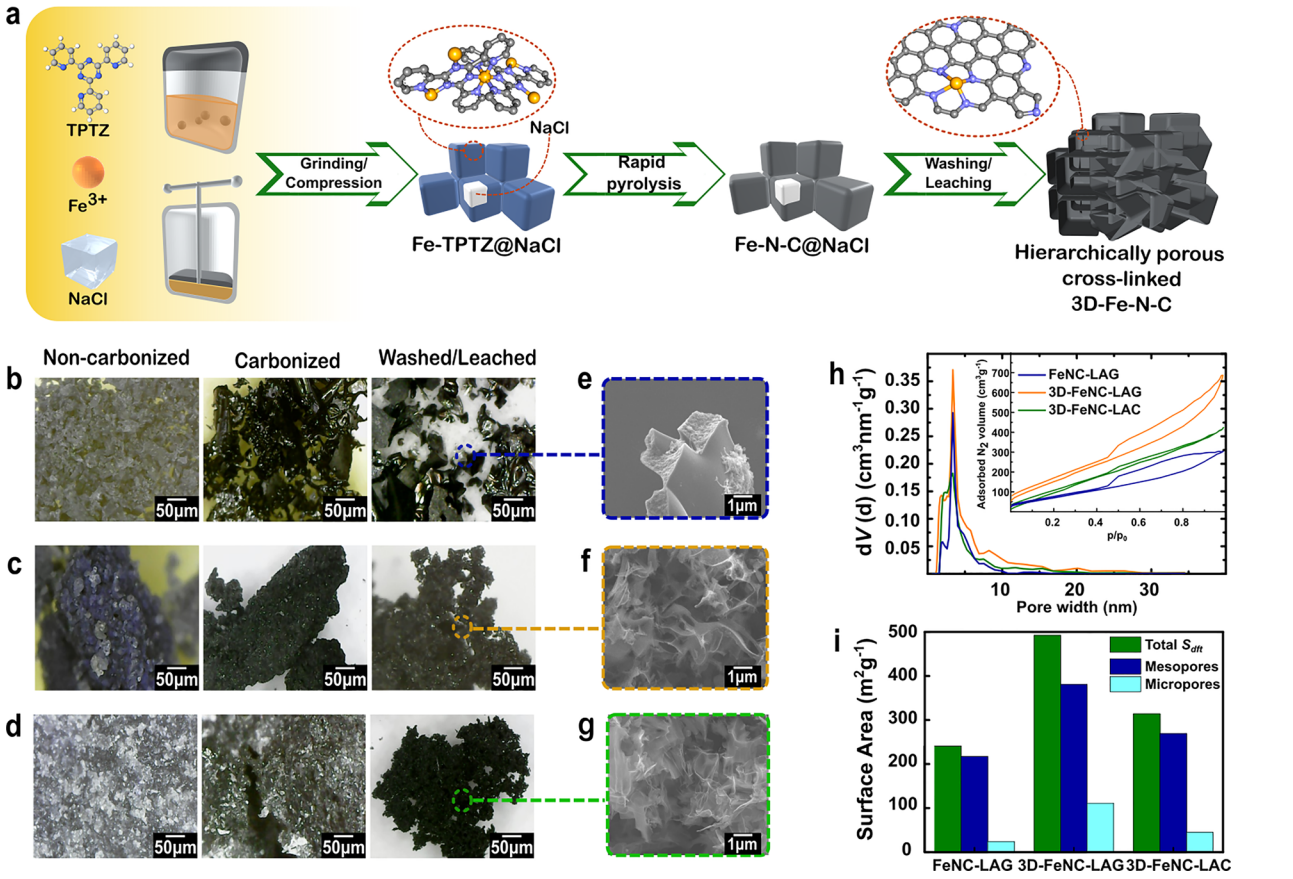

Figure 1. (a) Schematic illustration of catalyst synthesis via liquid-assisted grinding and liquid-assisted compression. (b–d) Microscope images of FeNC-LAG (b), 3D-FeNC-LAG (c), and 3D-FeNC-LAC (d) materials at various stages of synthesis. (e–g) SEM images of FeNC-LAG (e), 3D-FeNC-LAG (f), and 3D-FeNC-LAC (g) catalysts. (h) Pore size distribution curves and nitrogen adsorption–desorption isotherms (inset). (i) Pore surface area ratio.

tion, hydrothermal treatments, and wet impregnation/doping) pose sustainability concerns.[9] In particular, the formation of toxic waste, time/energy expenses, and excessive solvent use are liquid-phase-associated bottlenecks limiting large-scale production. Recently, solid-phase mechanosynthesis (MS) emerged as the most potent approach to tackle the M–N–C-related sustainability issues.[9] Unlike wet chemistry methods, mechanochemistry requires little-to-no solvents and often features straightforward resource-efficient protocols, resulting in waste minimization, improved scalability, and higher material output.[10] Recently, many reports have demonstrated the efficiency of MS by fabricating M–N–C-type materials, which outperformed PGM-based catalysts, reaching synthetic efficiency beyond solution-based protocols.[11] Additionally, the solid-phase synthesis serves as an adaptive ground to further improve the efficiency of M–N–C materials. Particularly, merging MS with the sacrificial templating method can boost the catalytic activity of M–N–C materials.[9] As highlighted by preceding studies, applying sacrificial templates effectively improves the porosity, mass/electron transport, and stability of M–N–Cs during pyrolysis.[12,13]

Despite the obvious advantages of solid-phase synthesis, the viability of industry-scale production of M–N–Cs is still hindered by the resource-intensive nature of the pyrolysis process required to effectively form the catalytic species.[14] The resulting high cost of M–N–C catalysts will significantly impact the total price of the ESC stack, as the catalyst constitutes a significant portion of the scaled-up ESC cost.[15] Additionally, in the overall viability assessment of ESC systems, identifying the catalyst production footprint remains an overlooked aspect of catalyst design–crucial to ensure the sustainability of ESC-derived energy.[16] To pioneer the sustainability assessment, related waste mapping, and cost-based efficiency of M–N–C synthesis, a multilayer stream mapping framework (MSM) was applied.[17] The MSM methodology was developed on the basis of innovative Lean methodologies to evaluate the resource efficiency of manufacturing systems.[18] The MSM analysis has undergone validation in various industrial sectors[19,20]–evolving into a modern digital leverage Lean tool. The MSM tool evaluates the efficiency of time and resource consumption in production systems, waste, and other variables in a given process, providing time-stamped, adaptable scorecards for easy mapping of inefficiency and waste hot spots. The MSM assessment serves as a strong foundation to confirm the viability of the M–N–C catalyst production.

This study addresses the aforementioned issues by developing a scalable energy-/time-efficient template-assisted mechanosynthesis of M–N–Cs and introducing the MSM approach as a robust tool for assessing the pre-industrial feasibility of catalyst synthesis. The MSM approach was applied to assess the sustainability of the developed protocol and to confirm its advantage over the recent mechanochemical synthetic routes. The synthesis method prioritizes ecofriendly, inexpensive materials ($FeCl_3$, TPTZ, and NaCl) and implements only water and ethanol as solvents. The synthesis is

https://doi.org/10.1021/acssuschemeng.3c02077
ACS Sustainable Chem. Eng. 2023, 11, 10825–10834

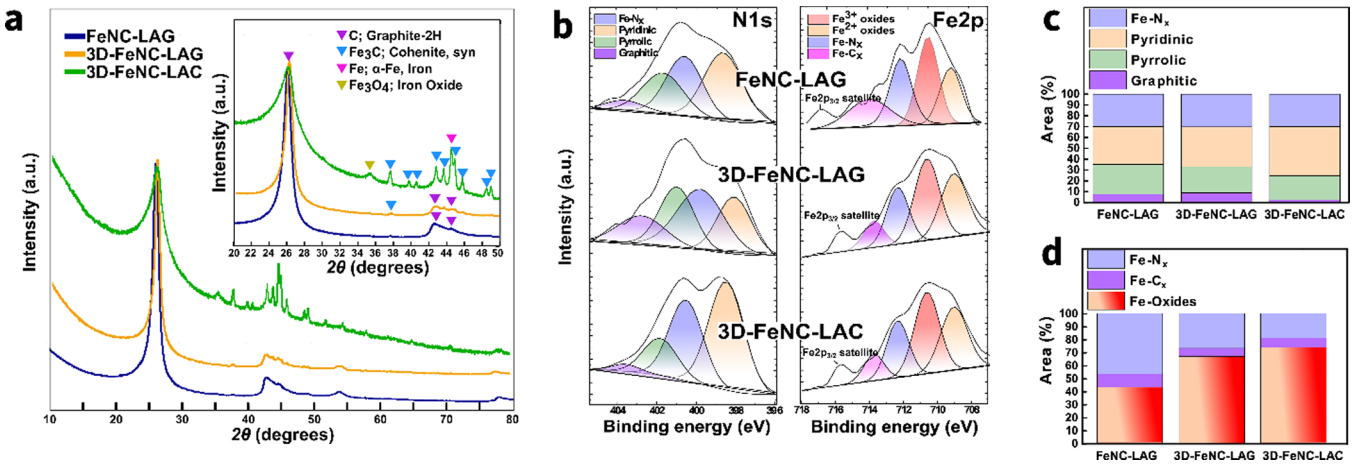

Figure 2. (a) XRD patterns of the samples FeNC-LAG, 3D-FeNC-LAG, and 3D-FeNC-LAC, with the inset showing a magnified region. (b) Deconvoluted high-resolution N 1s and Fe 2p photoelectron spectra of Fe−N−C catalysts. (c) Distribution of nitrogen species in Fe−N−C materials. (d) Distribution of iron species in Fe−N−C materials.

based on liquid-assisted grinding and compression techniques, using NaCl as an abundant and sustainable templating agent. Liquid-assisted grinding/compression leads to improved templating, enabling rapid pyrolysis and therefore improving the most energy-intensive step. The described approach yielded an efficient, bifunctional ORR/OER electrocatalyst−3D-FeNC-LAG, which exhibits promising catalytic activity in ORR ($E_{1/2}$ = 0.85 V, E_{onset} = 1.00 V) and OER ($E_{j=10}$ = 1.73 V). Furthermore, 3D-FeNC-LAG outperformed its commercially available counterparts in the Zn−air battery (power density of 139 mW cm^{-2} vs 120 mW cm^{-2} for PtRu). In terms of sustainability, the developed synthetic route stands out with its excellent cost/resource efficiency and minimal waste production (97.67% value-added cost) and thus a significantly reduced environmental footprint. The proposed method sets a new benchmark in M−N−C catalyst synthesis with at least 3 times less energy usage (4.3 vs 14.7+ kWh) and 2 times less processing time (5.6 vs 11+ h) compared to the prior methods. Furthermore, MSM was established as an effective tool for quantitative and detailed step-by-step process analysis−providing a road map for future improvements in the synthesis protocol. The current study encompasses the development of a sustainable synthesis protocol for the M−N−C catalyst and the implementation of a sustainability assessment tool using the proposed protocol as an example.

RESULTS AND DISCUSSION

Synthesis. This work employed an integrated approach of templated mechanosynthesis of a catalyst precursor to empower fast pyrolysis and yield the most energy-efficient production method for M−N−C-type catalysts (Figure 1a). Three different Fe−N−C catalysts were prepared by varying the synthetic conditions: FeNC-LAG, 3D-FeNC-LAG, and 3D-FeNC-LAC, where LAG stands for liquid-assisted grinding, LAC for liquid-assisted compression, and 3D identifies the application of the templating agent. Two different mechanosynthetic procedures−LAG and LAC, were applied to establish a correlation between the two methods and catalytic activity. To confirm the benefits of the NaCl support, the nontemplated catalyst FeNC-LAG was prepared via ball milling. 2,4,6-Tris(2-pyridyl)-1,3,5-triazine (TPTZ) ligand was employed as a carbon/nitrogen source with a high affinity toward coordinating to iron−forming Fe-TPTZ coordination polymers, where iron cations are better stabilized, less prone to clustering during pyrolysis, and stay as Fe−N$_x$ species.[7,12] To further improve the complex stability during rapid pyrolysis and increase the porosity and the concentration of active sites, a NaCl template was introduced through liquid-assisted mechanosynthesis.[12] Furthermore, NaCl, as a grinding aid, improves the efficiency of mechanosynthesis[21] and, when molten (Figure S1), acts as a highly polar solvent,[22] allowing Fe cations to coordinate with nitrogen species more effectively.

Characterization. Upon mechanochemical treatment, a distinct color change was observed from pale yellow to ink blue, confirming the structural change (Figure S2a), which was further confirmed by comparative PXRD (Figure S2b). Microscopy images of noncarbonized NaCl-supported catalysts in Figure 1c,d demonstrate the homogeneous inclusion of NaCl into the Fe−TPTZ framework, which is crucial in stabilizing Fe−TPTZ complexes during pyrolysis to improve the porosity and provide a better exposure to the catalytically active sites.[12] Upon washing and leaching, microscopy and SEM images of 3D-FeNC-LAG (Figure 1c,f) and 3D-FeNC-LAC (Figure 1d,g) demonstrate template-induced porous open-frame 3D structures, which would otherwise require additional carbon support in conventional synthetic methods.[23] In contrast, materials without NaCl support−FeNC-LAG−shows a dense and tightly arranged structure after washing/leaching (Figure 1b,e).

Similarly, the template-induced discrepancy in porosity was supported by the nitrogen gas adsorption−desorption analysis results. The produced Fe−N−C materials possess mixed nature, containing both micro- and mesopores. The adsorption−desorption isotherms in the inset of Figure 1h exhibit a Type IV hysteresis loop shape. Micropores and mesopores, which facilitate the charge and mass transfer,[24] were primarily distributed over the range of 1.2−2 and 2−34 nm, respectively (Figure 1h), with an average pore size of 3.42, 3.45, and 2.93 nm for FeNC-LAG, 3D-FeNC-LAG, and 3D-FeNC-LAC, respectively. BET analysis (Table S1) showed that among the samples, 3D-FeNC-LAG had the largest surface area S_{BET} = 563 m^2 g^{-1}, while FeNC-LAG and 3D-FeNC-LAC showed values of 269 and 430 m^2 g^{-1}, respectively.

Additionally, 3D-FeNC-LAG exhibited the highest concentration of micropores and mesopores (Figure 1i), which is crucial for catalysis.[25,26] Correlation between the surface area

https://doi.org/10.1021/acssuschemeng.3c02077
ACS Sustainable Chem. Eng. 2023, 11, 10825−10834

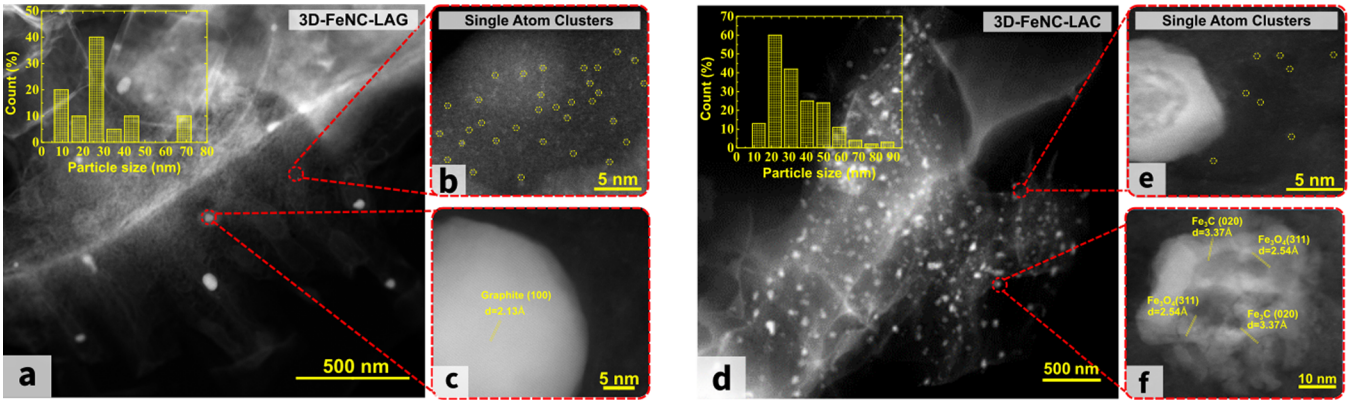

Figure 3. (a–c) STEM image of 3D-FeNC-LAG (a) with particle size distribution (a, inset) and magnified regions (b, c). (d–f) STEM image of 3D-FeNC-LAC (d) with particle size distribution (d, inset) and magnified regions (e, f).

and total pore volume was also evident, with 3D-FeNC-LAG having the largest pore volume of 0.97 $cm^3\ g^{-1}$, followed by 3D-FeNC-LAC (0.63 $cm^3\ g^{-1}$) and FeNC-LAG (0.46 $cm^3\ g^{-1}$).

Further, the surface content of the carbon-based material was analyzed to identify the atomic and nanoscale metal species and N-based moieties, which are the important factors for catalytic efficiency.[27,28] In PXRD analysis (Figure 2a), a peak at 26° (002) observed in each sample hints at the graphitic morphology of the materials.[29] Patterns of FeNC-LAG and 3D-FeNC-LAG show no significant peaks related to the iron species (elemental, oxide, and carbide). However, the bulk metal composition of FeNC-LAG and 3D-FeNC-LAG was identified as 0.960 and 1.471 wt% (Table S2), respectively, which hints the presence of either atomic dispersion of iron species or the formation of highly compacted agglomerates with very small particle sizes.[30] In contrast, compression-prepared 3D-FeNC-LAC showed the largest share of iron (9.3 wt % (Table S2)) and exhibited a collection of peaks related to various iron species at 44.3° (α-Fe), 35.5° (Fe_3O_4), and several peaks from 39° to 45° (Fe_3C) (inset in Figure 2a). While an overabundance of Fe/Fe_3C leads to the low accessibility of Fe–N_x sites,[31] the Fe/Fe_3C species can still contribute to 3D-FeNC-LAC ORR activity in a stepwise $2e^- \times 2e^-$ manner, forming peroxides and then decomposing them to water.[32,33] The low degree of graphitization and high concentration of Fe clusters in 3D-FeNC-LAC were attributed to insufficient homogeneity and energy during compression, as well as poor accessibility to metal clusters due to dense packing. This aspect of the synthetic protocol requires thorough optimization and will be addressed in further studies.

XPS measurements were performed to quantitatively determine the chemical surface composition of the catalysts. The atomic fractions of Fe, N, C, and O elements are summarized in Table S2. Deconvoluted high-resolution Fe 2p XPS spectra (Figure 2b) show the presence of four peaks at 714, 712, 710, and 709 eV, which are attributed to Fe–C_x, Fe–N_x, Fe^{3+}, and Fe^{2+} states, respectively.[34−37] According to the ratio of species in the N 1s region (Figure 2c), 30% of all N species are involved in the formation of Fe–N_x.

The iron species ratio depicted in Figure 2d indicates that FeNC-LAG constitutes the highest ratio of Fe–N_x among all three materials. However, the activity of these sites may be impeded by the low porosity of the FeNC-LAG sample, as it can lead to limited access to these sites.[24]

To better understand factors influencing the promising electrochemical performance of 3D-FeNC-LAG and 3D-FeNC-LAC (see Electrochemical Characterization section later in the text), the morphology of both samples was investigated using STEM. Images of 3D-FeNC-LAG (Figure 3a) reveal a high density of single atomically dispersed iron incorporated into the carbon matrix (Figure 3b) with a relatively small number of nanospecies with an average size of 27.35 nm (inset in Figure 3a). Figure 3c suggests that particles are confined in graphite (d = 2.13 Å, graphite (001)), forming graphene-wrapped nanoparticles, which have improved stability to oxidation and agglomeration.[11] Additionally, the synergic interaction between the nanoparticle core and carbon shell contributes to the overall performance by modulating the local electronic structure.[38,39] As expected, compression-derived 3D-FeNC-LAC demonstrates a considerably higher concentration of nanoparticles (Figure 3d) with a larger average size of 32.67 nm (inset in Figure 3d) and fewer single-atom sites (Figure 3e). To ascertain the nature of particles in 3D-FeNC-LAC, STEM (Figure 3f) and EDS elemental maps (Figure S3) were used, which further reveal that these nanoclusters are in the form of oxide-covered Fe_3C species surrounded by graphitic carbon layers. Despite the acceptable electrochemical activity of Fe_3C, it was observed that the overabundance of relatively large particles hinders the catalysis by lowering the accessibility of the active species and the synergic contribution of the porous N/C matrix.[31]

Electrochemical Characterization. The electrochemical activity of the catalysts was evaluated using a series of tests to determine how the structural properties and content of the catalysts affected their performance. The cyclic voltammetry (CV) technique was employed to investigate the capacitance and electrochemically active surface area of the materials. CV curves obtained for FeNC-LAG do not have any characteristic redox peaks (Figure S4), whereas 3D-FeNC-LAG and 3D-FeNC-LAC show broad oxidation peaks at 0.29 V vs RHE, which might be due to the contribution from the redox of the Fe^0/Fe^{3+} couple.[40] The double-layer capacitance (C_{DL}) measurements (Figure S5) show C_{DL} values of 2.7, 21.3, and 21.0 mF cm^{-2} for FeNC-LAG, 3D-FeNC-LAG, and 3D-FeNC-LAC, respectively. The acquired C_{DL} data were adjusted to electrode area ($S_{electrode}$ = 0.196 cm^2) to give the following adjusted C_{DL} values: FeNC-LAG C_{DL} = 0.529 mF, 3D-FeNC-LAG C_{DL} = 4.175 mF, and 3D-FeNC-LAC C_{DL} = 4.116 mF. Further, electrochemical active surface area (ECSA) values were quantitatively derived from C_{DL} (for details, see

https://doi.org/10.1021/acssuschemeng.3c02077
ACS Sustainable Chem. Eng. 2023, 11, 10825−10834

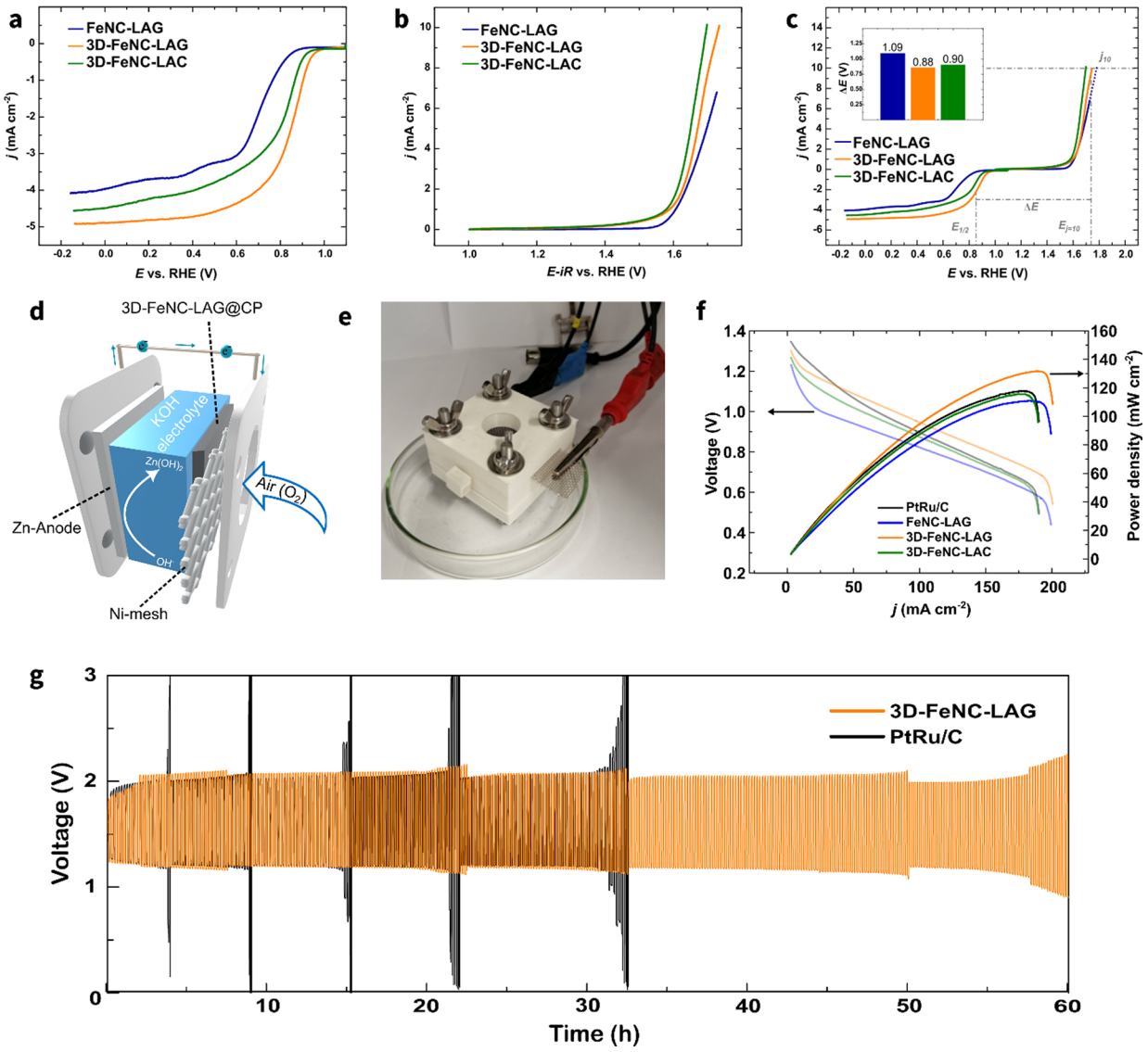

Figure 4. (a) ORR polarization curves of FeNC-LAG, 3D-FeNC-LAG, and 3D-FeNC-LAC in O_2-saturated 0.1 M KOH solution at a rotation rate of 1600 rpm. (b) OER polarization curves of FeNC-LAG, 3D-FeNC-LAG, and 3D-FeNC-LAC in Ar-saturated 0.1 M KOH solution at a rotation rate of 1600 rpm. (c) Overall polarization curves of FeNC-LAG, 3D-FeNC-LAG, and 3D-FeNC-LAC within the ORR and OER potential windows and the values of ΔE (c, inset). (d) Schematic illustration of a zinc−air battery. (e) Photograph of the assembled zinc−air battery. (f) Power density curves obtained for Fe−N−C and PtRu/C as catalysts on the air cathode (solid lines−power curves; hollow lines−−polarization curves). (g) Galvanostatic charge/discharge cycling curves for 3D-FeNC-LAG and PtRu/C materials (orange and black lines, respectively) performed at 5 mA cm^{-2}.

Supporting Information) as 13.2 cm^2 for FeNC-LAG, 104.4 cm^2 for 3D-FeNC-LAG, and 102.7 cm^2 for 3D-FeNC-LAC. The 3D-FeNC-LAG catalyst demonstrated the largest ECSA and C_{DL}, while FeNC-LAG showed the lowest of the three materials. Higher ECSA and C_{DL} values of templated materials suggest better active site exposure to the electrolyte, which can be attributed to the 3D structure of the templated materials. Additionally, the 3D structure can also improve the mass transport of reactants and products to and from the active sites, enhancing the electrocatalytic performance.[12]

Rotating disk electrode (RDE) studies were conducted on the prepared Fe−N−C samples to evaluate their ORR activity in an alkaline (0.1 M KOH) medium. ORR RDE polarization curves (Figure 4a) showed superior ORR activity for 3D-FeNC-LAG. The higher onset potential (E_{onset} = 1.00 V), half-wave potential ($E_{1/2}$ = 0.85 V), and larger limited current density (5.0 mA cm^{-2}) compared to FeNC-LAG and 3D-FeNC-LAC hint a better electron and mass transfer induced by higher porosity.[29,41] Furthermore, ORR Tafel analysis (Figure S6a) showed that 3D-FeNC-LAG has the lowest Tafel slope value (74 mV dec^{-1}), which implies the favorable ORR kinetics of 3D-FeNC-LAG. The Koutecky−Levich (K−L) plots (Figure S7) constructed from the ORR polarization curves at different rotation rates indicate primarily the $4e^-$ pathway for ORR on 3D-FeNC-LAG. The electron transfer numbers (n) for the three samples are shown in the insets of Figure S7. The RDE experiment results show that the 3D-FeNC-LAG sample has superior ORR activity compared to the other synthesized samples.

Further, the synthesized materials were evaluated for their ability to catalyze OER using linear sweep voltammetry (LSV) in a 0.1 M KOH solution under an argon-saturated

https://doi.org/10.1021/acssuschemeng.3c02077
ACS Sustainable Chem. Eng. 2023, 11, 10825−10834

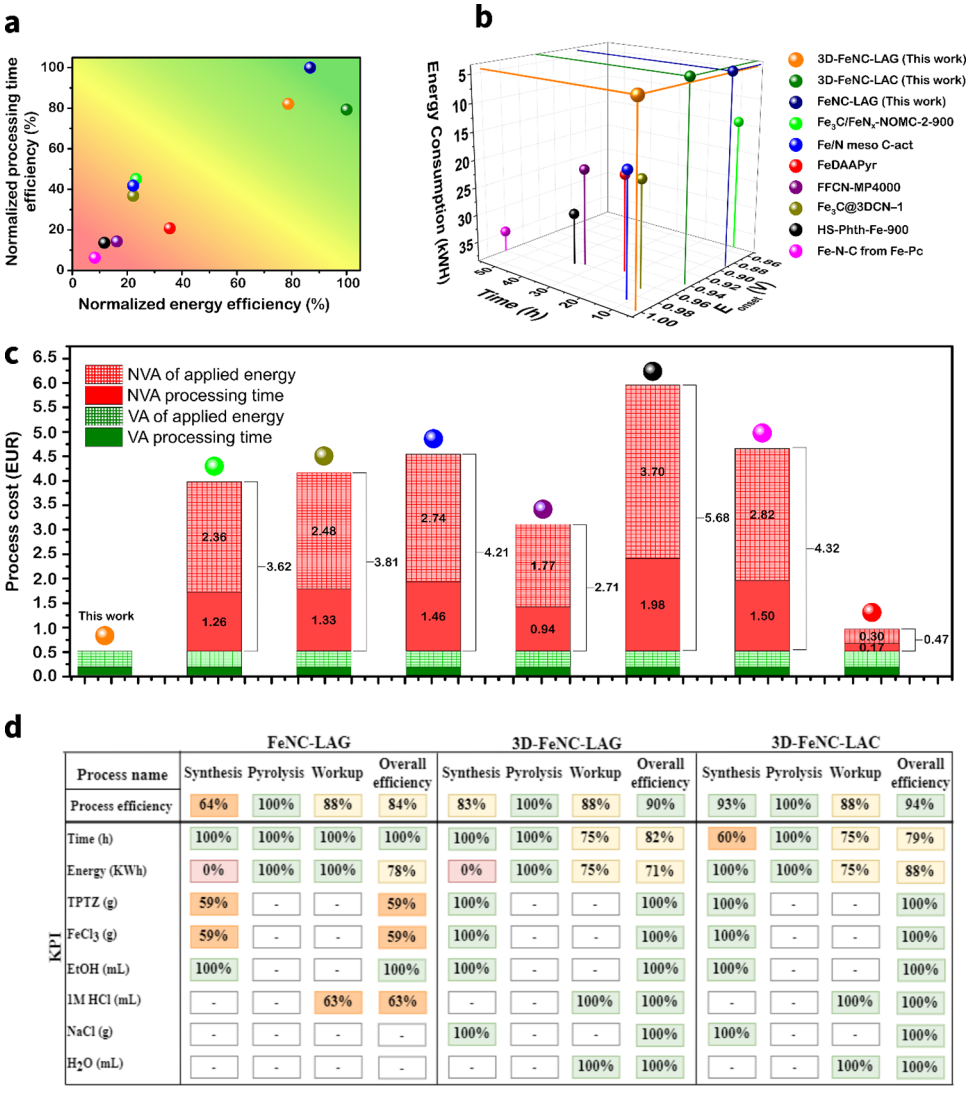

Process name	FeNC-LAG Synthesis	FeNC-LAG Pyrolysis	FeNC-LAG Workup	FeNC-LAG Overall efficiency	3D-FeNC-LAG Synthesis	3D-FeNC-LAG Pyrolysis	3D-FeNC-LAG Workup	3D-FeNC-LAG Overall efficiency	3D-FeNC-LAC Synthesis	3D-FeNC-LAC Pyrolysis	3D-FeNC-LAC Workup	3D-FeNC-LAC Overall efficiency
Process efficiency	64%	100%	88%	84%	83%	100%	88%	90%	93%	100%	88%	94%
Time (h)	100%	100%	100%	100%	100%	100%	75%	82%	60%	100%	75%	79%
Energy (KWh)	0%	100%	100%	78%	0%	100%	75%	71%	100%	100%	75%	88%
TPTZ (g)	59%	-	-	59%	100%	-	-	100%	100%	-	-	100%
$FeCl_3$ (g)	59%	-	-	59%	100%	-	-	100%	100%	-	-	100%
EtOH (mL)	100%	-	-	100%	100%	-	-	100%	100%	-	-	100%
1M HCl (mL)	-	-	63%	63%	-	-	100%	100%	-	-	100%	100%
NaCl (g)	-	-	-	-	100%	-	-	100%	100%	-	-	100%
H_2O (mL)	-	-	-	-	-	-	100%	100%	-	-	100%	100%

Figure 5. (a) Normalized energy and time consumption value comparison. (b) Correlation of energy and time efficiency with the catalytic activity in absolute values. (c) Value-added cost and non-value-added cost for the production of 1 g of the catalyst compared with the recently reported templated mechanosynthesis. (d) Scorecard for comparison of the process efficiency for FeNC-LAG, 3D-FeNC-LAG, and 3D-FeNC-LAC.

environment at the electrode rotation rate of 1600 rpm. The electrodes were scanned between the potential range of 1−1.8 V vs RHE to determine the potential required to reach the current density of 10 mA cm^{-2} ($E_{j=10}$). The LSV curves in Figure 4b indicate that the 3D-FeNC-LAC electrode exhibited the lowest $E_{j=10}$ value of 1.70 V, which was attributed to the abundance of OER-active nanoparticles on the surface of the electrode.[27]

The bifunctional activity of the prepared electrocatalysts was evaluated by determining the value of ΔE, which is calculated as the difference between $E_{j=10}$ and the $E_{1/2}$.[4] The results, presented in Figure 4c, reveal that the 3D-FeNC-LAG electrode exhibited the lowest ΔE value of 0.88 V, followed closely by 3D-FeNC-LAC with a value of 0.90 V. The obtained ORR and OER kinetic parameters for all three samples are summarized in Table S3.

The morphological characterization reveals that both the porosity of the material and the density of Fe−N_x sites are the essential contributors to the efficient oxygen bifunctionality of the material. As such, the lower bifunctional activity of FeNC-LAG can be attributed to the lower porosity, which decreases the wetting of the total surface, rendering a significant portion of the Fe−N_x sites inaccessible and, therefore, inactive.[42] The results demonstrate that the efficiency of 3D-FeNC-LAG and 3D-FeNC-LAC is comparable to that of the previously reported Fe−N−C catalysts, as seen in Table S4. However, it is essential to note that the previously reported liquid-phase protocols fall far behind in cost, energy efficiency, and overall sustainability compared to the proposed solid-phase synthesis approach.

Zinc-Air Battery Tests. Due to the superior bifunctional activity, 3D-FeNC-LAG was selected for further application in zinc−air batteries (ZABs). An in-house ZAB was constructed as a series of stacked plates (for details, see the Supporting Information), where the air cathode represents carbon paper-supported Fe−N−C catalysts (Figure 4d,e). As expected, 3D-FeNC-LAG demonstrated outstanding performance showing the highest power density among all three Fe−N−C catalysts (Table S5). The charge−discharge polarization curve revealed that ZAB driven by 3D-FeNC-LAG exhibits an open-circuit voltage of 1.30 V, comparable to that of the PGM-based reference material−PtRu/C (1.35 V). However, 3D-FeNC-

https://doi.org/10.1021/acssuschemeng.3c02077
ACS Sustainable Chem. Eng. 2023, 11, 10825−10834

LAG outperformed the PtRu/C catalyst, reaching a power density of 139 mW cm^{-2}, whereas the PtRu/C catalyst reached only 120 mW cm^{-2} (Figure 4f). Moreover, the power density of 3D-FeNC-LAG is comparable to the recent reports (Table S5).

Furthermore, the long-term performance of the catalyst material at the air cathode was evaluated through galvanostatic charge−discharge cycling measurements at a current density of 5 mA cm^{-2} (Figure 4g). During the stability test, the 3D-FeNC-LAG-driven battery demonstrated a steady voltage−time profile without significant fluctuations for 60 h, operating in the range of 1.52 V, maintaining a stable energy efficiency. Minor fluctuations are attributed to the formation of zinc dendrites, which lead to battery instability causing internal short circuits. Strategies to mitigate this shall be studied in a separate research work. In the same test, the PtRu/C catalyst started to dysfunction after only a few hours of work, constantly requiring refreshment of the entire battery setup. Significant voltage gaps between cycles (~2.4 V) observed in a PtRu/C-driven ZAB suggest a significantly lower stability of PGM-based setup compared to 3D-FeNC-LAG, which demonstrated only 0.45 V voltage gap between the first and last cycles (Figure S8). Important to note is that ZAB performance parameters also depend on the battery assembly and shall be addressed in a separate work. Nonetheless, the acquired results manifest the possibility of utilizing M−N−C catalysts produced via the proposed sustainable solid-state strategy.

Multilayer Stream Mapping Assessment. As previously reported, the synthetic efficiency of the proposed methodology goes far beyond the wet-chemistry protocols.[34] Although materials produced via liquid-based synthesis show excellent activity,[43−45] the solid-state synthetic approaches exhibit a distinct advantage in sustainability and demonstrate competitive performance as compared to the conventional solvent-based methods.[9,10,46] Therefore, to offer the most industrially suitable protocol, the grand challenge is to outperform the currently available solid-state approaches.

In this study, MSM was introduced to form the basis of technoeconomic and environmental upstream impact analysis of the catalyst production process. The MSM methodology was developed on the basis of innovative Lean methodologies; therefore, it is a tool for relative efficiency assessment, which allows establishing a benchmark among the compared processes.[17] To initiate the comparison, the MSM analysis requires determining the key performance indicators (KPIs)−process-associated parameters that can be compared. The KPIs (processing time, energy consumption, and E_{onset}) for the recently reported templating mechanosynthesis approaches are summarized in Table S6 (for estimation details, see the description in the table). The collected KPI functional units are defined per gram of the catalyst produced and expressed in h/g (time) and kWh/g (energy). E_{onset} was selected as a catalyst performance metric due to its ability to be precisely extracted from previous studies. Despite certain limitations in the completeness of the reported experimental data, the obtained data offer a comprehensive overview. The total energy consumption and processing time values from Table S6 were normalized, meaning that the best value in the set was established as 100%, and the remaining values were proportionally scaled relative to this benchmark. The results in Figure 5a show that the developed synthetic protocols exhibit over 80% relative time and energy efficiency, with at least 2 times faster processing time (5.6 vs 11+ h) and 3 times greater energy efficiency (4.3 kWh vs 14.7+ kWh) compared to the previously reported protocols (Table S6). Furthermore, to provide an all-encompassing perspective, the synthetic parameters of protocols (energy and time consumption) were correlated with the catalytic activity (E_{onset}). The estimated results in Figure 5b reveal that the synthesis of 3D-FeNC-LAG exhibits unprecedented energy and processing time efficiency while still retaining a high level of catalytic activity, displaying a marked superiority over the next best alternative−Fe/N meso act[47] (E_{onset} = 0.99 V, estimated energy consumption−16.8 kWh, and estimated processing time−11 h).

Furthermore, to map the process inefficiencies, MSM assessment was used to determine the value-added costs (VA)−representing the "useful consumption" that adds value to the process−and non-value-added costs (NVA)−representing the "waste/misuse" of time, energy, or resources.[17] To analyze the VA and NVA of solid-state protocols, a comparison of energy and time consumption of the pyrolysis step (the most representative and readily available data point) was selected. The functional units of this assessment represent time-related and energy-related costs expressed in EUR. For the time and energy cost assessment, refer to the Supporting Information. In Figure 5c, it is seen that the estimated VA of the proposed rapid pyrolysis is 100% (0.50 EUR), followed by the pyrolysis of FeDAAPyr[48] (estimated VA = 51% (0.50 EUR), and NVA = 49% (0.47 EUR)). Overall, the rapid pyrolysis facilitated by liquid-assisted templating in 3D-FeNC-LAG results in the lowest pyrolysis cost compared to other reports.

The MSM framework was further applied to evaluate the overall process efficiency of the proposed approaches. To investigate the efficiency of individual process steps and map necessary improvements, the scorecard (Figure 5d) was assembled according to MSM guidelines.[17,18] The scorecard shows the efficiency of the identified KPIs for the proposed protocols. KPIs for the proposed synthesis are summarized in Table S7 (for details, see the Supporting Information). The detailed information on the three developed protocols allows introducing the material-related cost (in EUR). MSM analysis reveals that despite the disparities in outcomes at individual steps, the overall efficiency of each protocol is over 80%. In the energy efficiency calculations, 100% efficiency of 3D-FeNC-LAC synthesis was achieved due to the manually operated hydraulic press. The quantification of energy expenditure in manual processes is more complex; therefore, it was assumed to be 0 kWh. On this account, the synthesis of 3D-FeNC-LAG resulted in low energy efficiency. However, industry-scale production prioritizes automated processing over manual labor to ensure safety, quality, and efficiency.[49] Thus, the 3D-FeNC-LAG production strategy stands out as the most industry-feasible among the proposed strategies, with an outstanding overall efficiency of 90%.

Furthermore, the VA and NVA of the syntheses were assessed. The estimation was performed based on laboratory-scale production, and it is anticipated that the cost of production will be significantly lower at the industrial scale.[50] The cost assessment of the FeNC-LAG protocol (Figure S10) shows that the nontemplated approach yields the lowest cost/resource efficiency. The largest non-value-added costs in the production process arise from the synthesis step (41.43%) and the workup step (31.46%), primarily due to the loss of TPTZ

https://doi.org/10.1021/acssuschemeng.3c02077
ACS Sustainable Chem. Eng. 2023, 11, 10825−10834

during carbonization and excessive utilization of HCl to eliminate large metal agglomerates. The cost of 1 g of FeNC-LAG was estimated around 16 EUR (for estimation, see the Supporting Information), out of which 39% (~6 EUR) is a misuse. On the contrary, these inefficiencies are effectively mitigated through the implementation of a more optimized template-assisted approach. The synthesis of 3D-FeNC-LAC and 3D-FeNC-LAG results in the lowest non-value-added cost (1.66 and 2.33%, respectively) and lower total price per 1 g of catalyst (~12 EUR) (Figures S11 and S12). Most of the "losses" are observed during the workup process (7.09% for both templated approaches), which requires additional time and energy to wash out the NaCl template. The acquired MSM data demonstrate that template-assisted mechanosynthesis improves the resource, energy, and cost efficiency of the process. Overall, the exceptional performance makes the proposed NaCl-templated liquid-assisted grinding protocol a benchmark in the area of transition-metal-based electrocatalyst synthesis, setting the standard for future developments in this field.

CONCLUSIONS

This study presents a novel approach to synthesizing Fe−N−C catalysts that are environmentally and economically advantageous. The described approach yields highly porous Fe/N-doped carbon materials with excellent bifunctional activity achieved through combining template-assisted mechanosynthesis and the NaCl sacrificial template. The promising electrochemical activity of 3D-FeNC-LAG toward ORR ($E_{1/2}$ = 0.85 V and E_{onset} = 1.00 V) and OER ($E_{j=10}$ = 1.73 V) and ZAB performance (a peak power density of 139 mW cm^{-2}) were achieved by the approach-induced high porosity (S_A = 563 m^2 g^{-1}) and high concentration of active sites (SAS/NPs). In terms of sustainability, the proposed method results in a reduced environmental footprint through accelerated processing (20 min per batch), improved resource efficiency, and minimized waste (97.67% value-added cost). NaCl template significantly lowers the energy consumption of pyrolysis−the most energy-intensive process step (1.82 vs 14.4 kWh on average (Table S7)). As a result, the proposed method requires at least 3 times less energy (4.3 vs 14.7+ kWh) and 2 times less processing time (5.6 vs 11+ h) compared to the prior methods. Overall, the developed synthesis approach and the established MSM sustainability analysis protocol will set a standard for the future holistic development and adaptation of M−N−C catalysts. Given the importance of sustainable energy in ensuring a greener future, the proposed template-assisted mechanosynthesis supports this transition by offering an economically feasible and sustainable synthesis strategy for fuel cells and MAB catalysts.

ASSOCIATED CONTENT

Supporting Information

The Supporting Information is available free of charge at https://pubs.acs.org/doi/10.1021/acssuschemeng.3c02077.

Materials and methods description; experimental procedure; XRD patterns of the Fe−TPTZ complex; SEM/EDS of Fe−N−C catalysts; calculation of reaction kinetic parameters; ZAB and AEMFC performance; MSM KPI summary and calculations; and process cost assessment calculation (PDF)

AUTHOR INFORMATION

Corresponding Author

Nadezda Kongi − *Institute of Chemistry, University of Tartu, 50411 Tartu, Estonia;* orcid.org/0000-0001-9680-0421; Email: nadezda.kongi@ut.ee

Authors

Akmal Kosimov − *Institute of Chemistry, University of Tartu, 50411 Tartu, Estonia*

Amina Alimbekova − *Institute of Chemistry, University of Tartu, 50411 Tartu, Estonia*

Jurgen-Martin Assafrei − *Institute of Chemistry, University of Tartu, 50411 Tartu, Estonia*

Gulnara Yusibova − *Institute of Chemistry, University of Tartu, 50411 Tartu, Estonia*

Jaan Aruväli − *Institute of Ecology and Earth Sciences, University of Tartu, 50411 Tartu, Estonia*

Maike Käärik − *Institute of Chemistry, University of Tartu, 50411 Tartu, Estonia*

Jaan Leis − *Institute of Chemistry, University of Tartu, 50411 Tartu, Estonia;* orcid.org/0000-0002-3352-5909

Päärn Paiste − *Institute of Ecology and Earth Sciences, University of Tartu, 50411 Tartu, Estonia*

Majid Ahmadi − *Faculty of Science and Engineering, University of Groningen, 9747 AG Groningen, The Netherlands;* orcid.org/0000-0003-2321-3060

Khatereh Roohi − *Department Materials Science and Engineering, Delft University of Technology, 2628 CD Delft, The Netherlands*

Peyman Taheri − *Department Materials Science and Engineering, Delft University of Technology, 2628 CD Delft, The Netherlands*

Sara M. Pinto − *INEGI − Institute of Science and Innovation in Mechanical and Industrial Engineering, 4200-465 Porto, Portugal*

Ritums Cepitis − *Institute of Chemistry, University of Tartu, 50411 Tartu, Estonia*

Antonio J. Baptista − *INEGI − Institute of Science and Innovation in Mechanical and Industrial Engineering, 4200-465 Porto, Portugal*

Patrick Teppor − *Institute of Chemistry, University of Tartu, 50411 Tartu, Estonia*

Enn Lust − *Institute of Chemistry, University of Tartu, 50411 Tartu, Estonia*

Complete contact information is available at: https://pubs.acs.org/10.1021/acssuschemeng.3c02077

Notes

The authors declare no competing financial interest.

ACKNOWLEDGMENTS

The present work was financially supported by the Estonian Research Council (grant nos PSG250 and PRG1509). This research was also supported by the EU through the European Regional Development Fund (TK141, "Advanced materials and high-technology devices for energy recuperation systems").

REFERENCES

(1) Bhoyate, S. D.; Kim, J.; de Souza, F. M.; Lin, J.; Lee, E.; Kumar, A.; Gupta, R. K. Science and Engineering for Non-Noble-Metal-Based Electrocatalysts to Boost Their ORR Performance: A Critical Review. *Coord. Chem. Rev.* **2023**, *474*, No. 214854.

(2) Wang, Y.; Pang, Y.; Xu, H.; Martinez, A.; Chen, K. S. PEM Fuel Cell and Electrolysis Cell Technologies and Hydrogen Infrastructure Development − a Review. *Energy Environ. Sci.* **2022**, *15*, 2288−2328.
(3) Yang, C.; Xia, J.; Cui, C.; Pollard, T. P.; Vatamanu, J.; Faraone, A.; Dura, J. A.; Tyagi, M.; Kattan, A.; Thimsen, E.; Xu, J.; Song, W.; Hu, E.; Ji, X.; Hou, S.; Zhang, X.; Ding, M. S.; Hwang, S.; Su, D.; Ren, Y.; Yang, X.-Q.; Wang, H.; Borodin, O.; Wang, C. All-Temperature Zinc Batteries with High-Entropy Aqueous Electrolyte. *Nat. Sustainability* **2023**, *6*, 325−335.
(4) Xu, H.; Yang, J.; Ge, R.; Zhang, J.; Li, Y.; Zhu, M.; Dai, L.; Li, S.; Li, W. Carbon-Based Bifunctional Electrocatalysts for Oxygen Reduction and Oxygen Evolution Reactions: Optimization Strategies and Mechanistic Analysis. *J. Energy Chem.* **2022**, *71*, 234−265.
(5) Wang, Y.; Zheng, X.; Wang, D. Design Concept for Electrocatalysts. *Nano Res.* **2022**, *15*, 1730−1752.
(6) Zeng, K.; Zheng, X.; Li, C.; Yan, J.; Tian, J.-H.; Jin, C.; Strasser, P.; Yang, R. Recent Advances in Non-Noble Bifunctional Oxygen Electrocatalysts toward Large-Scale Production. *Adv. Funct. Mater.* **2020**, *30*, No. 2000503.
(7) Shi, Z.; Yang, W.; Gu, Y.; Liao, T.; Sun, Z. Metal-Nitrogen-Doped Carbon Materials as Highly Efficient Catalysts: Progress and Rational Design. *Adv. Sci.* **2020**, *7*, No. 2001069.
(8) Du, C.; Gao, Y.; Wang, J.; Chen, W. A New Strategy for Engineering a Hierarchical Porous Carbon-Anchored Fe Single-Atom Electrocatalyst and the Insights into Its Bifunctional Catalysis for Flexible Rechargeable Zn−Air Batteries. *J. Mater. Chem. A* **2020**, *8*, 9981−9990.
(9) Peera, S. G.; Liu, C. Unconventional and Scalable Synthesis of Non-Precious Metal Electrocatalysts for Practical Proton Exchange Membrane and Alkaline Fuel Cells: A Solid-State Co-Ordination Synthesis Approach. *Coord. Chem. Rev.* **2022**, *463*, No. 214554.
(10) James, S. L.; Adams, C. J.; Bolm, C.; Braga, D.; Collier, P.; Friščić, T.; Grepioni, F.; Harris, K. D. M.; Hyett, G.; Jones, W.; Krebs, A.; Mack, J.; Maini, L.; Orpen, A. G.; Parkin, I. P.; Shearouse, W. C.; Steed, J. W.; Waddell, D. C. Mechanochemistry: Opportunities for New and Cleaner Synthesis. *Chem. Soc. Rev.* **2012**, *41*, 413−447.
(11) Wen, G.-L.; Niu, H.-J.; Wang, A.-J.; Yin, Z.-Z.; Zhang, Q.-L.; Feng, J.-J. Graphene Wrapped Fe7C3 Nanoparticles Supported on N-Doped Graphene Nanosheets for Efficient and Highly Methanol-Tolerant Oxygen Reduction Reaction. *J. Colloid Interface Sci.* **2019**, *556*, 352−359.
(12) Guo, C.; Zhou, R.; Li, Z.; Si, Y.; Liao, W.; Sun, W.; Xiang, S.; Luo, X.; Luo, M.; Luo, Z. Molten-Salt/Oxalate Mediating Fe and N-Doped Mesoporous Carbon Sheet Nanostructures towards Highly Efficient and Durable Oxygen Reduction Electrocatalysis. *Microporous Mesoporous Mater.* **2020**, *303*, No. 110281.
(13) Hu, J.; Wu, D.; Zhu, C.; Hao, C.; Xin, C.; Zhang, J.; Guo, J.; Li, N.; Zhang, G.; Shi, Y. Melt-Salt-Assisted Direct Transformation of Solid Oxide into Atomically Dispersed FeN4 Sites on Nitrogen-Doped Porous Carbon. *Nano Energy* **2020**, *72*, No. 104670.
(14) Zhang, S.; Jiang, S.-F.; Huang, B.-C.; Shen, X.-C.; Chen, W.-J.; Zhou, T.-P.; Cheng, H.-Y.; Cheng, B.-H.; Wu, C.-Z.; Li, W.-W.; Jiang, H.; Yu, H.-Q. Sustainable Production of Value-Added Carbon Nanomaterials from Biomass Pyrolysis. *Nat. Sustainability* **2020**, *3*, 753−760.
(15) Fan, L.; Deng, H.; Zhang, Y.; Du, Q.; Leung, D. Y. C.; Wang, Y.; Jiao, K. Towards Ultralow Platinum Loading Proton Exchange Membrane Fuel Cells. *Energy Environ. Sci.* **2023**, *16*, 1466.
(16) Usai, L.; Hung, C. R.; Vásquez, F.; Windsheimer, M.; Burheim, O. S.; Strømman, A. H. Life Cycle Assessment of Fuel Cell Systems for Light Duty Vehicles, Current State-of-the-Art and Future Impacts. *J. Cleaner Prod.* **2021**, *280*, No. 125086.
(17) Peças, P.; Gonçalves, B.; Rocha, B.; Jorge, D.; Baptista, A. Optimization techniques to support decision-making processes via MSM—an Industry 4.0 approach. In *Advances in Mathematics for Industry 4.0*; Ram, M., Ed.; Academic Press, 2021; pp 23−60.
(18) Lourenço, E. J.; Baptista, A. J.; Pereira, J. P.; Dias-Ferreira, C. Multi-Layer Stream Mapping as a Combined Approach for Industrial Processes Eco-Efficiency Assessment. In *Re-engineering Manufacturing for Sustainability*; Nee, A. Y. C., Song, B., Ong, S.-K., Eds.; Springer: Singapore, 2013; pp 427−433.
(19) Gomes, M. N.; Baptista, A. J.; Guedes, A. P.; Ribeiro, I.; Lourenço, E. J.; Peças, P. Multi-Layer Stream Mapping: Application to an Injection Moulding Production System. In *Sustainable Design and Manufacturing 2017*; Campana, G., Howlett, R. J., Setchi, R., Cimatti, B., Eds.; Smart Innovation, Systems and Technologies; Springer International Publishing: Cham, 2017; pp 193−202.
(20) Baptista, A. J.; Lourenço, E. J.; Peças, P.; Silva, E. J.; Estrela, M. A.; Holgado, M.; Benedetti, M.; Evans, S. MAESTRI Efficiency Framework as a Support Tool for Industrial Symbiosis Implementation. In *WASTES − Solutions, Treatments and Opportunities II*; CRC Press, 2017.
(21) Yang, J.; Feng, X.; Lu, G.; Li, Y.; Mao, C.; Wen, Z.; Yuan, W. NaCl as a Solid Solvent to Assist the Mechanochemical Synthesis and Post-Synthesis of Hierarchical Porous MOFs with High I2 Vapour Uptake. *Dalton Trans.* **2018**, *47*, 5065−5071.
(22) Menga, D.; Ruiz-Zepeda, F.; Moriau, L.; Šala, M.; Wagner, F.; Koyutürk, B.; Bele, M.; Petek, U.; Hodnik, N.; Gaberšček, M.; Fellinger, T. Active-Site Imprinting: Preparation of Fe−N−C Catalysts from Zinc Ion−Templated Ionothermal Nitrogen-Doped Carbons. *Adv. Energy Mater.* **2019**, *9*, No. 1902412.
(23) Zhao, X.; Pachfule, P.; Li, S.; Simke, J. R. J.; Schmidt, J.; Thomas, A. Bifunctional Electrocatalysts for Overall Water Splitting from an Iron/Nickel-Based Bimetallic Metal−Organic Framework/Dicyandiamide Composite. *Angew. Chem., Int. Ed.* **2018**, *57*, 8921−8926.
(24) Dash, R. K.; Yushin, G.; Gogotsi, Y. Synthesis, Structure and Porosity Analysis of Microporous and Mesoporous Carbon Derived from Zirconium Carbide. *Microporous Mesoporous Mater.* **2005**, *86*, 50−57.
(25) Macchi, S.; Denmark, I.; Le, T.; Forson, M.; Bashiru, M.; Jalihal, A.; Siraj, N. Recent Advancements in the Synthesis and Application of Carbon-Based Catalysts in the ORR. *Electrochemistry* **2022**, *3*, 1−27.
(26) Jaouen, F.; Lefèvre, M.; Dodelet, J.-P.; Cai, M. Heat-Treated Fe/N/C Catalysts for O_2 Electroreduction: Are Active Sites Hosted in Micropores? *J. Phys. Chem. B* **2006**, *110*, 5553−5558.
(27) Zhang, K.; Zou, R. Advanced Transition Metal-Based OER Electrocatalysts: Current Status, Opportunities, and Challenges. *Small* **2021**, *17*, No. 2100129.
(28) Zha, S.; Wang, D.; Liu, C.; Wang, W.; Mitsuzaki, N.; Chen, Z. Heteroatom Doped M−N−C Single-Atom Catalysts for High-Efficiency Oxygen Reduction Reaction: Regulation of Coordination Configurations. *Sustainable Energy Fuels* **2022**, *6*, 3895−3906.
(29) Lyu, D.; Mollamahale, Y. B.; Huang, S.; Zhu, P.; Zhang, X.; Du, Y.; Wang, S.; Qing, M.; Tian, Z. Q.; Shen, P. K. Ultra-High Surface Area Graphitic Fe-N-C Nanospheres with Single-Atom Iron Sites as Highly Efficient Non-Precious Metal Bifunctional Catalysts towards Oxygen Redox Reactions. *J. Catal.* **2018**, *368*, 279−290.
(30) Zhang, J.; Chen, J.; Luo, Y.; Chen, Y.; Luo, Y.; Zhang, C.; Xue, Y.; Liu, H.; Wang, G.; Wang, R. A Defect-Driven Atomically Dispersed Fe−N−C Electrocatalyst for Bifunctional Oxygen Electrocatalytic Activity in Zn−Air Batteries. *J. Mater. Chem. A* **2021**, *9*, 5556−5565.
(31) Chen, Z.; Gao, X.; Wei, X.; Wang, X.; Li, Y.; Wu, T.; Guo, J.; Gu, Q.; Wu, W. D.; Chen, X. D.; Wu, Z.; Zhao, D. Directly Anchoring Fe3C Nanoclusters and FeNx Sites in Ordered Mesoporous Nitrogen-Doped Graphitic Carbons to Boost Electrocatalytic Oxygen Reduction. *Carbon* **2017**, *121*, 143−153.
(32) Kim, J. H.; Sa, Y. J.; Jeong, H. Y.; Joo, S. H. Roles of Fe−N_x and Fe−Fe_3C@C Species in Fe−N/C Electrocatalysts for Oxygen Reduction Reaction. *ACS Appl. Mater. Interfaces* **2017**, *9*, 9567−9575.
(33) Hu, E.; Yu, X.-Y.; Chen, F.; Wu, Y.; Hu, Y.; Lou, X. W. D. Graphene Layers-Wrapped Fe/Fe_5C_2 Nanoparticles Supported on N-Doped Graphene Nanosheets for Highly Efficient Oxygen Reduction. *Adv. Energy Mater.* **2018**, *8*, No. 1702476.
(34) Kosimov, A.; Yusibova, G.; Aruväli, J.; Paiste, P.; Kärik, M.; Leis, J.; Kikas, A.; Kisand, V.; Šmits, K.; Kongi, N. Liquid-Assisted

Grinding/Compression: A Facile Mechanosynthetic Route for the Production of High-Performing Co−N−C Electrocatalyst Materials. *Green Chem.* **2022**, *24*, 305−314.
(35) Xiao, T.; Wang, Y.; Wan, J.; Ma, Y.; Yan, Z.; Huang, S.; Zeng, C. Fe-N-C Catalyst with Fe-NX Sites Anchored Nano Carboncubes Derived from Fe-Zn-MOFs Activate Peroxymonosulfate for High-Effective Degradation of Ciprofloxacin: Thermal Activation and Catalytic Mechanism. *J. Hazard. Mater.* **2022**, *424*, No. 127380.
(36) Xu, Y.; Chen, B.; Nie, J.; Ma, G. Reactive Template-Induced Core−Shell FeCo@C Microspheres as Multifunctional Electrocatalysts for Rechargeable Zinc−Air Batteries. *Nanoscale* **2018**, *10*, 17021−17029.
(37) Peng, H.; Mo, Z.; Liao, S.; Liang, H.; Yang, L.; Luo, F.; Song, H.; Zhong, Y.; Zhang, B. High Performance Fe- and N- Doped Carbon Catalyst with Graphene Structure for Oxygen Reduction. *Sci. Rep.* **2013**, *3*, 1765.
(38) Bandal, H. A.; Pawar, A. A.; Kim, H. Transformation of Waste Onion Peels into Core-Shell Fe3C@ N-Doped Carbon as a Robust Electrocatalyst for Oxygen Evolution Reaction. *Electrochim. Acta* **2022**, *422*, No. 140545.
(39) Weng, W.; Zhou, J.; Gu, D.; Xiao, W. Thermoelectrochemical Formation of Fe/Fe $_3$ C@hollow N-Doped Carbon in Molten Salts for Enhanced Catalysis. *J. Mater. Chem. A* **2020**, *8*, 4800−4806.
(40) Osmieri, L.; Escudero-Cid, R.; Monteverde Videla, A. H. A.; Ocón, P.; Specchia, S. Performance of a Fe-N-C Catalyst for the Oxygen Reduction Reaction in Direct Methanol Fuel Cell: Cathode Formulation Optimization and Short-Term Durability. *Appl. Catal., B* **2017**, *201*, 253−265.
(41) Zhong, L.; Jiang, C.; Zheng, M.; Peng, X.; Liu, T.; Xi, S.; Chi, X.; Zhang, Q.; Gu, L.; Zhang, S.; Shi, G.; Zhang, L.; Wu, K.; Chen, Z.; Li, T.; Dahbi, M.; Alami, J.; Amine, K.; Lu, J. Wood Carbon Based Single-Atom Catalyst for Rechargeable Zn−Air Batteries. *ACS Energy Lett.* **2021**, *6*, 3624−3633.
(42) Jiang, W.-J.; Gu, L.; Li, L.; Zhang, Y.; Zhang, X.; Zhang, L.-J.; Wang, J.-Q.; Hu, J.-S.; Wei, Z.; Wan, L.-J. Understanding the High Activity of Fe−N−C Electrocatalysts in Oxygen Reduction: Fe/Fe $_3$ C Nanoparticles Boost the Activity of Fe−N_x. *J. Am. Chem. Soc.* **2016**, *138*, 3570−3578.
(43) Bai, L.; Duan, Z.; Wen, X.; Guan, J. Bifunctional Atomic Iron-Based Catalyst for Oxygen Electrode Reactions. *J. Catal.* **2019**, *378*, 353−362.
(44) He, J.; Zheng, T.; Wu, D.; Zhang, S.; Gu, M.; He, Q. Insights into the Determining Effect of Carbon Support Properties on Anchoring Active Sites in Fe−N−C Catalysts toward the Oxygen Reduction Reaction. *ACS Catal.* **2022**, *12*, 1601−1613.
(45) Chen, G.; Liu, P.; Liao, Z.; Sun, F.; He, Y.; Zhong, H.; Zhang, T.; Zschech, E.; Chen, M.; Wu, G.; Zhang, J.; Feng, X. Zinc-Mediated Template Synthesis of Fe-N-C Electrocatalysts with Densely Accessible Fe-Nx Active Sites for Efficient Oxygen Reduction. *Adv. Mater.* **2020**, *32*, No. 1907399.
(46) Cuccu, F.; De Luca, L.; Delogu, F.; Colacino, E.; Solin, N.; Mocci, R.; Porcheddu, A. Mechanochemistry: New Tools to Navigate the Uncharted Territory of "Impossible" Reactions. *ChemSusChem* **2022**, *15*, No. e202200362.
(47) Toyama, Y.; Miyake, K.; Shu, Y.; Moroto, K.; Ma, J.; Zheng, T.; Tanaka, S.; Nishiyama, N.; Fukuhara, C.; Kong, C. Y. Solvent-Free Synthesis of Fe/N Doped Hierarchal Porous Carbon as an Ideal Electrocatalyst for Oxygen Reduction Reaction. *Mater. Today Energy* **2020**, *17*, No. 100444.
(48) Serov, A.; Artyushkova, K.; Andersen, N. I.; Stariha, S.; Atanassov, P. Original Mechanochemical Synthesis of Non-Platinum Group Metals Oxygen Reduction Reaction Catalysts Assisted by Sacrificial Support Method. *Electrochim. Acta* **2015**, *179*, 154−160.
(49) Singh, S.; Namekar, S. A review on automation of industries. *Int. J. Eng. Appl. Sci. Technol.* **2020**, *04*, 298−300.
(50) Mankiw, N. G. *Principles of Economics*, 7th ed.; Cengage Learning: USA, 2014.

https://doi.org/10.1021/acssuschemeng.3c02077
ACS Sustainable Chem. Eng. 2023, 11, 10825−10834